

Sobinov and Yakovenko

Analytical solution of a bilateral Brown-type central pattern generator for symmetric and asymmetric locomotion

Short title: Analytical solution of CPG model

Anton Sobinov¹ and Sergiy Yakovenko^{1,2*}

¹ Centers for Neuroscience, School of Medicine, West Virginia University, Morgantown, WV, USA

² Division of Exercise Physiology, Department of Human Performance, School of Medicine, West Virginia University, Morgantown, WV, USA

* Corresponding author

E-mail: seyakovenko@hsc.wvu.edu (SY)

Sobinov and Yakovenko

Abstract

The coordinated activity of muscles is produced in part by spinal rhythmogenic neural circuits termed the central pattern generators (CPGs). A classical CPG model proposed conceptually by T.G. Brown in 1911 is a system of coupled oscillators transforming locomotor drive into coordinated and gait-specific patterns of muscle recruitment. A system of ordinary differential equations with physiologically inspired coupling locus of interactions captures the timing relationship for the bilateral coordination of limbs in locomotion and is typically solved numerically. Consequently, it is intriguing to have a full analytical description of this plausible CPG architecture to illuminate the functionality within this structure. Here, we provided a closed form analytical solution contrasted against the previous numerical method. The computational load of the analytical solution was decreased by an order of magnitude compared to the comparable numerical approach (with relative errors $<0.01\%$). The analytical solution tested and supported the previous finding that the input to the model can be expressed in the units of the desired limb locomotor speed. Furthermore, we performed the parametric sensitivity analysis in the context of controlling asymmetric locomotion and documented two possible mechanisms associated either with an external drive or the intrinsic CPG parameters. The results support the idea that many different combinations of network states even within the same anatomical structure of CPG may generate the same behavioral outcomes.

Sobinov and Yakovenko

Author Summary

Using a simple process of leaky integration, we have developed an analytical solution to a robust model of the spinal pattern generation. We have analyzed the ability of this neural element to exert locomotor control with the signal associated with limb speeds, which represent high-level modality within the motor system. Furthermore, we tested the ability of this simple structure to embed the steering control using the velocity signal in model's inputs or within the internal connectivity of its elements. Both mechanisms can produce the same behavioral outcome, which points to the methodological challenges of modeling CPGs and demonstrates the possibility of spinal circuit adaptations to asymmetric short- or long-term conditions in health and disease.

Sobinov and Yakovenko

Introduction

Specialized neural elements in the spinal cord, the central pattern generators (CPGs), contribute to the generation of periodic coordinated patterns of locomotor activity (1). Discovered in deafferented preparations, CPGs do not require sensory signals to produce locomotor behavior; however, their pattern is greatly influenced by sensory and descending inputs (2,3). Specifically, the direct electrical stimulation of a brainstem structure called the mesencephalic locomotor region (MLR) even in decerebrated animals produces oscillations in the CPGs and subsequent locomotor behavior (4). This locomotor behavior is characterized by the complex coordinated actions of multiple muscle groups. It is remarkable that the change in either magnitude or frequency of MLR stimulation can generate all appropriate modifications of these patterns. The increase in stimulation expresses a full repertoire of gaits with continuous transitions from walking to trotting, and galloping in over-the-ground locomotion (5), or causes the transition from slow walking to swimming in amphibians (6), which is a faster than walking mode of locomotion. Thus, the increase of stimulation input current corresponds to the increase in locomotor velocity.

Many CPG models were developed over the last century (7-13). Simulated model structure and its parameters are usually derived from observing the motor output patterns or their changes in response to external inputs or naturally occurring variations. These models give rise to the mechanistic descriptions that capture biological organization and the processes; however, they generally start as phenomenological or statistical representations of observed phase variations or timing in the recorded muscle activity. For example, both limb-based Brown's CPG (14) and joint-based Grillner's CPG (15) are similarly founded on the observations of multiple representative electromyographic (EMG) profiles providing insight into the functional organization of this circuitry.

The idea of CPG as a distributed mechanism that integrates convergent inputs (4) has been supported by both computational and experimental studies. Using calcium imaging, the spatiotemporal activity of rhythmogenic circuitry was found to be functionally distributed together with the motoneurons in the rostral lumbar and sacral segments of the spinal cord (16,17). The spatiotemporal distribution of neural activity throughout the lumbar enlargement with descending control and sensory inputs intact was visualized by combining the anatomical location of motoneurons with the information about their activity during normal locomotion (18). This was also supported by the observations of independent and coupled recruitment of flexor and extensor rhythmogenic spinal circuits using selective optogenetic approaches (19). The rhythmogenesis in only flexors or only extensors with the optogenetics supports the computational observation of switch-like transition between flexors and extensors (or more precisely, limb protractors and retractors), which identifies them as distinct network elements (18). This bilateral switch-like activation of the motor pools spanning the full rostrocaudal extent of the lumbosacral enlargement is likely associated with the distributed rhythm-generating networks responsible for this activity.

The integration of feedforward predictions and sensory feedback about ongoing execution is the optimal solution for generating robust control of complex body morphology (20). Over the course of evolution, the process of optimization within the control pathways has likely been concerned with the optimization of locomotion, as the central behavior essential for animal survival (2). One engineering solution to the problem of computing predictive commands for complex systems is the use of inverse models (21,22). The complex transformation from muscle activations into the movement kinematics could be internalized for inverse solutions that generate appropriate output for the desired kinematic input. It is then not surprising that the dedicated rhythmogenic networks for locomotion may be embedding the dynamics of body-ground interactions to solve the problems of intra- and interlimb coordination (13,23). The accuracy of these embedded neural calculations of musculoskeletal transformation may be fine-tuned by experience (24-27). It is important to

Sobinov and Yakovenko

acknowledge that sensory feedback pathways may also shape the final output of motor pathways and compensate for the dynamics during locomotion. In addition, there is considerable evidence that CPG integrates sensory inputs together with supraspinal commands to generate changes in timing and magnitude of locomotor activity (2,28).

The models of CPG offer a unique research opportunity to understand the interplay between these neural directives and biomechanical constraints that govern a complex dynamic task. To this extent, we have previously used inverse solutions of a CPG model to infer the nature of descending inputs (2). The surprising result of simulations was that the input to CPG was the velocity of each limb. Described mathematically as a system of differential equations (2,10,29-32), the CPG models are hard or even impossible to solve analytically in the form of known functions and variables. Still, the analytical expressions have several advantages over the numerical models. Unlike numerical solutions that often suffer from the accumulating errors and inversely related computational load, the analytical solutions are precise within assumptions taken during their derivation. They are also evaluated expressed more efficiently and are faster than the approximate numerical solutions.

In this study, we developed a method to obtain an analytical solution to one of the simplest implementations of locomotor CPG. We used this analytical expression to test further the ability of this circuitry to embed the regulation of phases appropriate for different speeds and to control steering with asymmetric gaits. While the identification of pattern generating elements remains to be a considerable challenge in experimental techniques, the function of distributed elements of CPG can be probed with the computational methods that allow us to monitor and manipulate any part of the circuit. We test two hypotheses in this study: 1) the exact analytical solution exists for the bilateral CPG model implemented with the leaky integration process; 2) the intrinsic circuit redundancy in CPG can accommodate the expression of asymmetric gait. The function of embedding the asymmetric representations of gait may be relevant for understanding steering and short- and long-term adaptations within the spinal systems.

Methods

Model description

While a few CPG models of neural activity consider specific ion dynamics using Hodgkin-Huxley formulation (10,32), our model captures gross CPG network dynamics described by T.G. Brown in a form of gated leaky integration. We expressed the input-output relationship using coupled leaky integrators formulated as a system of ordinary differential equations (ODEs). The system of ODEs can be expressed in matrix form (Eq. 1) with ipsilateral antagonism expressed as abrupt non-overlapping state transitions. The event associated with any given state x_i value crossing 1 triggers the resetting of the state to 0 and the start of integration for the ipsilateral antagonist. In Fig 1, for example, if the left flexor (x_1) reaches 1, it resets to 0 and turns off, while left extensor (x_2) switches on.

Equation 1

$$\dot{x} = U_0 + G_u u + G_l x + Gx$$

where: $x = (x_1, x_2, x_3, x_4)^T$ - state vector, U_0 - constant input from intrinsic connections, G_u - extrinsic input gains, u - extrinsic inputs, G_l - leak gains, G - weights for connections between integrators (r_{ff} , r_{fe} , r_{ef} , r_{ee} weights in Fig 1).

Fig 1. Schematic of the bilateral locomotor CPG model.

Sobinov and Yakovenko

The oscillatory behavior in each half-center (marked 1-4) was generated through the intrinsic leaky integrate-to-threshold resetting. This process was also under regulation from intrinsic inputs governed by parameters (r_{ff} , r_{fe} , r_{ef} , r_{ee}). The flexor half-centers (blue) were reciprocally connected to extensor half-centers (red). See Eq. 1-2 for details.

To simplify model parameter space, the parameters were coupled assuming symmetrical organization across the midline as seen in Eq. 2. Additionally, the connection between flexors (r_{ff}) was removed for simulations of walking behavior, where swing phases do not overlap.

Equation 2

$$U_0 = \begin{pmatrix} u_{of} \\ u_{oe} \\ u_{of} \\ u_{oe} \end{pmatrix}, G_u = \begin{pmatrix} g_{uf} \\ g_{ue} \\ g_{uf} \\ g_{ue} \end{pmatrix}, G_l = \begin{pmatrix} g_{lf} \\ g_{le} \\ g_{lf} \\ g_{le} \end{pmatrix} \cdot I, G = \begin{pmatrix} 0 & 0 & r_{ef} \\ 0 & r_{fe} & r_{ee} \\ r_{fe} & r_{ee} & 0 \end{pmatrix}.$$

We used fixed-step 4th order Runge-Kutta method with 10^{-3} s precision for forward numerical integration.

Analytical solution

The bilateral CPG model produces flexor (swing) and extensor (stance) phases for two limbs in relation to extrinsic input and intrinsic structure. To obtain these phases, Eq. 1 needs to be integrated in time between the state changes. Numerical integration was previously used (2) to generate swing and stance periods. The same transition points can be calculated analytically by transforming Eq. 1 into a matrix Cauchy problem:

Equation 3

$$\begin{cases} \dot{x} - Ax = B \\ x(t=0) = x_0 \end{cases}$$

where $A=G_l+G$ represents intrinsic structure of the CPG, $B=U_0+G_u u$ represents state-independent inputs, and x_0 is the initial condition. In case of a non-singular matrix A , this system has a vector form solution:

Equation 4

$$x = A^{-1}(e^{At} - I)B + e^{At}x_0$$

where I is the identity matrix. This analytical expression of states x (with dimensionality [4x1] for the model of bilateral CPG) describes the progression of all locomotor phases in time between the state changes. The remaining task is then to calculate the transition times and corresponding phase durations for a full step cycle. Eq. 4 was evaluated for all three possible bilateral combinations of concurrent flexor-extensor activity during a full step cycle, namely: i) left flexion and right extension (states x_1 and x_4), ii) left extension and right extension (states x_2 and x_4), and iii) left extension and right flexion (states x_2 and x_3). States may have repeated more than once within the step cycle, when CPG activity was highly asymmetric. The dimensionality of the problem can be reduced from 4 to 2 because only two integrators are active at any given time with the following parameters:

Equation 5

$$A = \begin{pmatrix} a_{ii} & a_{ij} \\ a_{ji} & a_{jj} \end{pmatrix}, B = \begin{pmatrix} b_i \\ b_j \end{pmatrix}, x_0 = \begin{pmatrix} x_{oi} \\ x_{oj} \end{pmatrix}$$

Sobinov and Yakovenko

where $i \in \{1, 2\}$ and $j \in \{3, 4\}$ are the indices of the two active integrators. We can then find the time of phase transitions τ for a given integrator k by inserting the reduced parameter set (Eq. 5) into Eq. 4, and assuming x_i or x_j equal to 1. Solving for τ yields the following transcendental equation:

Equation 6

$$z_1 \cdot \cosh(q\tau) + z_2 \cdot \frac{\sinh(q\tau)}{q} = z_3 \cdot e^{-s\tau}$$

where z_1, z_2, z_3, s, q are parameters describing the model configuration. The τ was then found numerically using Brent's method and analytically by expanding hyperbolic functions using Maclaurin series. We used NumPy 'roots' function (33) to solve the polynomials of power over 2. Next, the periods of activity of flexors and extensors during a step cycle were obtained with the following iterative algorithm:

- i. Calculate the time τ_i when state x_i reaches 1.
- ii. Calculate the time τ_j when state x_j reaches 1.
- iii. Calculate the state of all integrators at time point $\tau = \min(\tau_i, \tau_j)$.
- iv. Reset state from 1 to 0, deactivate it, and activate reciprocal ipsilateral state. For example, switch from active left flexor to activate left extensor.
- v. If full step cycle is completed (all 4 states reached value 1 at least once), stop; otherwise, go to step 1.

Cost function

The CPG model can generate multiple locomotor behaviors as a function of extrinsic inputs and its intrinsic interactions (2). Given a desired behavior, e.g. stereotypical symmetrical walking (34), the appropriate CPG parameters were found by optimizing the cost function (Eq. 7) that expressed the goodness of fit between target (experimental) and simulated patterns. In the symmetrical model, we optimized for 6 different speeds from 0.1 to 1.5 m/s (dashed lines in Fig 2) that were generated with 6 values of u (evenly distributed between 0.1 and 1.5 au). Fig 2 shows the quality of simulated solutions for a symmetrical walking over the full range of walking speeds.

Fig 2. Experimental and simulated locomotor phase duration characteristic.

Top: The relationship between locomotor phase and step cycle durations is shown with points representing the superimposed numerical and analytical solutions that are highly correlated with the experimental data lines, flexor (blue) and extensor (red) phases (34). *Bottom:* The corresponding simulated speed (black points) is plotted as a function of step duration and compared to experimental solution (black line) (see Fig 3, in (35)).

Equation 7

$$J_c = k_1 H + k_2 M + k_3 O + k_4 C$$

where H is the difference of simulated and experimental stance and swing periods. The experimental periods were calculated using a best-fit formula obtained empirically (34). M is the difference of simulated and desired speed ranges that promotes the converging on nontrivial solutions. O is the cost associated with the erroneous co-activation of contralateral flexors. C is the degree of asymmetry between the simulated speeds of left and right limbs. All function components were normalized to produce values approximately between 0 and 1, relative weights $(k_1, k_2, k_3, k_4) = (1, 0.7, 2, 0.4)$. C and M components were removed in simulations intended to produce asymmetrical gait (see Fig 6 & 7 in Results).

Sobinov and Yakovenko

Optimization and parameter perturbation

Globally optimal set of parameters was found numerically using a combination of basin-hopping algorithm (36) in SciPy (37), and several constrained local minimizers: non-linear optimization algorithm COBYLA (38), truncated Newton algorithm (39), L-BFGS-B algorithm (40), and Powell's method (38). *First*, the global optimal parameter set (z^*) was found. In the optimization, the starting value for basin-hopping was obtained from the brute force search over the complete parameter space. Then the other algorithms optimized sequentially to arrive at the optimal solution ($z^* = \text{argmin}(Jc)$). *Second*, we created a normal multivariate distribution to evaluate the nature of close-to-optimal solutions. For this, the distribution was defined by the mean at z^* and the covariance matrix with the diagonal elements set to $0.01z^*$, or the equivalent of standard deviation set at 1% value of the optimal solution. The dataset of 10^5 points was then drawn from this distribution and used in the comparison between analytical and numerical solutions in Fig 3A. *Third*, the intermediate solutions of the first step corresponding to local minima were selected to determine the full functional range of parameters in the model, excluding sets with large cost values ($Jc > 10$). The adjusted for symmetry range for each parameter is shown as the span of y-axes in Fig 4. *Fourth*, we used a uniform distribution across the symmetrical full range of parameters to create another dataset of 10^5 values for the analysis of the expanded range comparison shown in Fig 3BC. *Fifth*, we created the parameter dataset perturbed by 10% from z^* . Similar to step 2 above, we created the normal multivariate distribution with the mean at z^* and the covariance diagonal elements set to $0.1z^*$. *Sixth*, we drew randomly 40 starting seeds and tasked the basin-hopping algorithm (set to 200-iterations for each seed) to repeat the optimization using one of the four local optimization algorithms. This final step in the analysis generated 160 optimal sets for all local algorithms in our analysis. The comparison of parametric distributions is shown for a third of best solutions in Fig 4. The cut of solutions was necessary to reject expected minimization failures with non-converging searches or those terminating with large cost function values.

Phenomenological models of locomotion

We used several phenomenological models created to describe the relationships between different parameters of stepping during locomotion in our analysis. The relationships between stance and swing phases relative to the cycle duration were taken from the study of Halbertsma (34). The relationship between step cycle duration (T_c) and velocity (V) was taken from the study of Goslow et al. (1973), where $V = (1.84 \cdot T_c)^{-1.68}$ (see Fig 2, bottom) (35). Both studies used best-fit functions to describe data from a small sample of cats; yet, these relationships have been recently confirmed with a large subject pool (41).

In the analysis of asymmetrical locomotion, we introduced a simple geometrical relationship for walking on a curve. The turn radius of an asymmetric bipedal walk (Eq. 8) was expressed as a function of hip width (L) and an asymmetry parameter $\alpha = V_{\text{left}}/V_{\text{right}}$:

Equation 8

$$R = \frac{L}{|\alpha - 1|}$$

The corresponding heading direction change during a single step can then be stated as:

Equation 9

$$\gamma = \arctan\left(\frac{V_{\text{right}} - V_{\text{left}}}{L} T_c\right),$$

where γ denotes the heading direction angle from forward direction; T_c - full step cycle period.

Sobinov and Yakovenko

Results

Comparison of analytical and numerical solutions

In this study, the continuous dynamics between phase transitions was demonstrated with a simple CPG model expressed as a system of interacting oscillators and solved either numerically or analytically using an iterative algorithm (Eq. 4). These analytical solutions were validated in simulations producing the experimentally observed periods of flexor and extensor activations in overground locomotion (for example, see Fig 2). The model was further extended to analyze asymmetric gait and to test the ability of this circuit to embed asymmetric gait control.

High-precision numerical approach carries the processing cost that usually exceeds that of analytical methods. Fig 3 shows the comparison of processing cost between numerical and analytical solutions for this model (Eq. 1). The error of evaluating phase transitions with the numerical method (blue line) and the analytical solutions using the root-finding algorithm (red line) was the same at the precision for numerical integration set to 10^{-3} s (intersection marked with *, Fig 3 AB). The analytical solutions to Eq. 4 found by expanding hyperbolic terms, linear to the 9th power, are shown with shades of gray in Fig 3. Here, the difference between analytical and numerical estimations of the time of phase transitions was evaluated with the root mean square (RMS) metric of simulation quality. Shown in Fig 3A, the quadratic approximation (gray line marked with 2) provided similar quality to the analytical solutions (red line) with sets of close-to-optimal parameters (in 1% vicinity of the optimal set, see step two in section “Optimization and parameter perturbation” in Methods). When the model parameters were chosen randomly from the full range of feasible parameters (steps three and four in Methods), quadratic solutions did not provide desirable precision and performed worse than the numerical method, with other powers only approaching a reasonable threshold of over 10 ms error (Fig 3B), which is the order of a motor unit action potential.

Fig 3C shows that the analytical solution was the best choice for precise real-time applications of this model outperforming the numerical method by close to an order magnitude. However, if the estimation errors of over 10 ms are insignificant in a specific application, e.g. using EMG-driven simulations with aggressive low-pass filtering, then the high orders of analytical approximations could provide appropriate solutions with even lower computational load than the full analytical solution. The approximations of powers 3-9 use eigenvalue approach to find roots of polynomials, which is relatively costly, but still more precise than some of the comparable numerical integrators.

Fig 3. The comparison of analytical and numerical solutions.

The measures of numerical (blue), analytical (red), and analytical approximations of different orders (shades of gray with order numbers) are plotted as functions of numerical precision, where dashed line indicates most relevant for real-time simulations precision of 1 ms. **A.** Full cycle error in the estimation of phase transition times using the 1% neighborhood of the optimal solution. Because the higher orders of approximations provide the same high precision as the cubic approximations, powers τ^4 - τ^9 are not displayed. **B.** Similar to **A**, the errors are shown for the random distribution of parameters. **C.** Average CPU time needed to calculate a full step period of 1.25 s (average from Halbertsma’s equations) in Python/NumPy implementation. The data presented in all subplots was averaged over 10^5 trials.

Sobinov and Yakovenko

Parametric sensitivity

A perturbation analysis was used to investigate the parametric sensitivity of suboptimal solutions that satisfy Eq. 7. This analysis compared optimal values found by several different local minimization methods after a 10% normal parametric perturbation (for details, see steps five and six in section “Optimization and perturbation” of Methods). From 160 solutions, 33% with the lowest J_c were: 30 by COBYLA, 1 by L-BFGS-B, 22 by Powell's algorithm, 2 by Truncated Newton's (TNC). COBYLA and Powell's algorithms, provided 95% of the best solutions in this problem. The distribution of parameters in Fig 4 with similar cost (J_c) across all methods indicates that the similar outputs could be produced with disparate circuit parameters. The parameters in the model were differently conserved across similar solutions: the input weights (G_u) had lower variability relative to other parameters, i.e. the static leak (x_0), static input (u_0), and interlimb connection weights (green, r_{ij}).

Fig 4. Analysis of parameter sensitivity.

The distributions of model parameters and cost function (J_c) are shown for the selection of best optimization sets. Each subplot shows a mean with standard deviation of the parameter values in blue (flexor), red (extensor), and green (mixed) for 4 types of the minimization algorithms. Except for cost function subplot, the vertical axis range reflects the full feasible range of parameters as determined by the examination of intermediate solutions (see step six in section “Optimization and parameter perturbation” of Methods) in subplots indicates the full possible parametric range (with the exception for the J_c values).

Behavioral implications of CPG morphology

The velocity hypothesis states that the descending signals to the CPG are the desired speeds of each leg. We wanted to test further if the analytical solution to the ODEs would produce the same or different velocity prediction for the modality of inputs. The direct relationship between the descending input and the temporal characteristics of stepping (step cycle, swing, and stance durations) was extracted from the second-order solution to Eq. 6. Although it has a complex non-linear form (Eq. 10), its combination with the solution from Goslow et al. (1973) for the relationship between step cycle period and forward velocity produced a linear result shown in Fig 5 ($r^2=0.999$, $p<0.001$ for left and right limbs).

Equation 10

$$V = \left(\frac{k_1 + k_2 u}{k_3 - \sqrt{k_4 + k_5 u}} + k_6 \right)^{1.68}$$

where k_i are configuration-dependent constants, u is descending input, and V is the forward velocity of locomotion.

Fig 5. The relationship between the simulated CPG command signal to each limb and the forward velocity.

The analytical solution for the full step cycle was calculated over the set of 10 input values for each limb (u). Each value produced simulated step cycle duration values, which was then plotted as forward velocity calculated with the experimental relationship from Goslow et al. (1972) for each limb. The identity ($y=x$) is plotted in black.

Sobinov and Yakovenko

We further explored the role of this descending command for velocity regulation in the generation of asymmetric gait. The asymmetric patterns were simulated by uncoupling the gains for left and right inputs of both flexors and extensors ($g_{uf1}, g_{ue1}, g_{uf2}, g_{ue2}$) in Eq. 2 and varying them independently by 33% of the optimal parameter set (Table 1). C and M components responsible for the pattern symmetry and simulated velocity related errors were removed from the cost function (Eq. 7) in this analysis. The simulated speed of walking for left and right limb was then calculated from the generated bilateral phases (Fig 6). The parameter asymmetry led to a steady gradient of the speed differences ($\alpha = V_{left}/V_{right}$, see Methods).

Table 1. Optimal model parameters. The parameter set (z^*) for Eq. 2 that satisfies Eq. 7.

x_{of}	x_{oe}	g_{uf}	g_{ue}	g_{lf}	g_{le}	u_{of}	u_{oe}	r_{fe}	r_{ef}	r_{ee}
0.244	0.376	1.59	2.62	-0.689	0.828	2.26	-0.174	-0.025	2.38	0.418

Fig 6AB show that variation of both inputs (g_{uf}, g_{ue}) together can produce asymmetric walking $\alpha=1.1$, with the turn diameter to be as low as 10 m (calculated from Eq. 8, or heading direction $\gamma=10^\circ$ change per step, see Eq. 9). Only the parameter combinations corresponding to the continuous gradient around the midline produced appropriately accurate simulations with low J_c , see Fig 6B. Uncoupled inputs to flexors and extensors can similarly generate asymmetric gaits with α up to 1.2 ($\gamma=20^\circ$). The gradient of cost for extensors was orthogonal to that for flexors in Fig 6DF, the increased possible range of asymmetric speeds was associated with the increased cost, as indicated in Fig 6B, with the cost trough extending along the diagonal unity.

Fig 6. External inputs generate asymmetric gait in the model.

The coupled and uncoupled input gain parameters (g_{ue}, g_{uf}) were related to the velocity asymmetry (Left panels) with the corresponding cost function outputs (Right panels). **AB**. The input gains of flexors and extensors were varied together for each limb. **CD**. Only flexor input gains (left and right g_{uf}) were manipulated for each limb. **EF**. Only extensor input gains (left and right g_{ue}) were manipulated for each limb. Inserts in **B** indicate the steering direction for two selected parameter sets.

Fig 7 shows that the intrinsic parameters in the model can also produce asymmetric gaits. Symmetric connections (e.g. in Eq. 2, $r_{fe}=r_{14}=r_{41}$) were uncoupled ($r_{14}\neq r_{41}$) and varied independently. As in the analysis above, α and J_c were calculated for the parameter variations of up to $\pm 33\%$ of the optimal value. The connections from flexor to contralateral extensor did not provide a suitable gradient of asymmetric walking speeds in the explored range of parameters (Fig 7A). Possible reasons for that are a low magnitude of the optimal value for this parameter (r_{ef} in Table 1) and the near constant relationship between swing duration and locomotor velocity (Fig 2). The variation of extensor-to-flexor and extensor-to-extensor parameters (r_{ef}, r_{ee}) produced asymmetric gaits (Fig 7CE) with the turn diameter of 10 m (heading direction $\gamma=10^\circ$ per step). These were comparable to the above result obtained from the analysis of external inputs. The profile of J_c was different for the gaits generated by variation of r_{ee} and r_{ef} parameters (Fig 7DF). The extensor-to-flexor parameter r_{ef} increased steering angle with a smaller increase in cost (Fig 7F) than compared to the extensor-to-

Sobinov and Yakovenko

extensor parameter r_{ee} (Fig 7D). However, r_{ee} could regulate asymmetric gaits over a larger range of velocities than r_{ef} as indicated by the diagonally extending trough in the cost function in Fig 7F.

Fig 7. Intrinsic parameters generate asymmetric gait in the model.

The uncoupled intrinsic parameters (r_{fe} , r_{ef} , r_{ee}) were related to the velocity asymmetry (*Left panels*) with the corresponding cost function outputs (*Right panels*). **AB**. The flexor-to-extensor weights (r_{fe}). **CD**. The extensor-to-flexor weights (r_{ef}). **EF**. The extensor-to-extensor weights (r_{ee}).

Discussion

In this study, we have developed a novel analytical description of a simple CPG model for locomotor phase timing and further expanded our previous model (9) to include not only externally-driven asymmetric rhythmogenesis but also the opportunity to internalize this asymmetric transformation within the structure of CPG. Our three central results are i) the model can be solved analytically; ii) the analytical solution converges on the same conclusion that the input to CPG is in the modality of limb forward velocity; iii) the minimalistic model of CPG built with coupled oscillating leaky integrators offers multiple opportunities for embedding asymmetric control.

What is the goal of using analytical solutions of neurophysiological models? The numerical solutions are usually the preferred option of solving complex models. For example, a biophysical CPG model proposed by Rybak et al. (2006) captures neurological basis of activity in detail, often using hundreds of approximated parameters and their reconfiguration during failures in the motor execution (10). Complex models with multiple estimated transformations may produce ensemble behavior that reproduces the expected outcome; however, the role of elements and their network properties are hard to predict and to analyze. Unlike models that are not analytically solvable, the simple models are often insightful and capable of identifying specific targets that modify circuit behavior (42-44). For example, in the study of Barnett and Cymbalyuk (2014) the saddle-node bifurcation of equilibria was manipulated to design rhythmogenic regimes with appropriate timing and phase duration characteristics (42). The employed bifurcation control method relies on the manipulation of a controlling parameter near a transition between different regimes responsible for spiking and bursting properties. Spardy et al. (2011) showed how the dynamical system analysis could identify the silent and bursting periods of system's oscillation, the effect of sensory inputs on the range of behavior, and the operation of CPG model in response to simulated spinal cord injury (45). This description was based on the simplified model (11,46) that uses two types of neuron implementations consisting of one- or two-dimensional differential equations for a single limb flexor-extensor CPG. Similar to other much more complex implementations, e.g. (10,47,48), even this simplified formulation produces a challenging system of equations for 10 neurons with 33 connections between them. The model did noticeably have problems resolving locomotor phases for the fast cycle durations (less than 800 ms, see Fig 3 in (46)). In contrast, our simple model had only 4 parameters within a reciprocally connected system of 2 leaky integrators, and it simulated the same behavior without the aberrations at the extremes of experimental data (9). This basic that we extended in this study was used to describe, for the first time, the novel flexibility of extensor- and flexor-dominant phase regulation.

As in other models, we were concerned that expanding the model's parametric space to describe two limbs could have introduced the uncontrollable increase in the errors associated with the corresponding parametric explosion. The bilateral half-centers for two limbs required a system of 4 differential equations and the set of either 7 coupled (see Eq. 2) or 16 uncoupled intrinsic and 4 extrinsic (input) parameters. Then the result for the expanded model in Fig 2 showing phase modulation over the full range of walking velocities without the limitations at the extremes was not

Sobinov and Yakovenko

a forgone conclusion. Overall, the increased parametric complexity in the model did not lead to the overfitting problem that could have appeared from estimating too many parameters from a low-dimensional set of behavioral data. Instead, the model consistently converged on similar solutions without the loss of validity indicated by the cost function.

Overfitting and underfitting are two major concerns in the selection of appropriate level of abstraction for models (49). In the words of John von Neumann, "With four parameters I can fit an elephant and with five I can make him wiggle his trunk." Here, our simple model relies on 20 parameters to generate low-dimensional output in the form of the phase characteristic in normal and asymmetric locomotion. Models based on Hodgkin-Huxley (H-H) formalism could generate the same phase duration characteristic; albeit, with the use of a large model parameter sets that extend into hundreds and thousands. Remarkably, the solutions from these two different representations are similar, which is supporting the experimental and computational observations that the same network activity could be generated by the underlying disparate mechanisms (48,50-52). Still, the convergence of our parameter search on the physiological network solution is validated only by the constraining behavioral data and the extent of simulated validation using parameter sensitivity analysis. Even in this minimalistic model, the exploration of 20-dimensional parameter space was challenging and led us to implement the analysis of a coupled symmetrical model first, where the parameters representing spinal neural elements mirrored across the midline were set to the same values. The perturbations in each parameter achieved with different minimization algorithms produced robust solutions where small changes did not lead to large changes in outcome (Fig 4). Thus, the model may not be overfitting for these particular phenomena under study.

Embedding of asymmetric gait control in extrinsic and intrinsic parameters

Even in our relatively simple model, there is a complicated relationship between intrinsic connections and extrinsic inputs. An indication of this fact is the capacity for representing the same behavior within parameters corresponding to different anatomical structures. Thus, it was necessary to uncouple the parameters in Eq.2 to further extend the sensitivity analysis with the goal of exploring the functionality "hidden" in the complexity to generate falsifiable hypotheses or model predictions.

We chose asymmetric gait as the test task because it results from the normal control of steering or heading direction (2,53), and it may contain indicators of long-term adaptations to injury. First, we "forced" the model to internalize the control of asymmetric stepping by changing only extrinsic parameters. The mechanism using only input gains of flexor half-centers, and less so of extensor half-centers, was a robust method of changing the interlimb speed differential. This was also expressed as the change in the heading direction in this model. In Fig 6, the tuning of input gains to flexor half-centers led to the asymmetric speed ratios of 0.9 to 1.1, which corresponds to the estimated heading direction change of $\pm 10^\circ$ over one step cycle (about 10 m turn diameter). This suggests that a single external input representing a heading direction could generate the realistic range of asymmetric gaits in this model. Second, we can similarly constrain the solution to the locus of intrinsic parameters responsible for the influences among four half-centers in the model. In studies of spinal segmental connectivity, these parameters would correspond to the 'gains' of propriospinal pathways connecting rhythmogenic networks within the spinal enlargement (54). It was intriguing to see the capability of this model to embed the asymmetric processing within these pathways. Moreover, the simulations suggested that not all parameters are equal targets in that respect. The extensor-to-flexor and extensor-to-extensor (r_{ef} , r_{ee} in Fig 7) parameters embedded the ability to generate asymmetric gaits with the reasonable turn diameter of 10 m. It is likely that steeper turning would require the contribution of additional hip strategies (55). Overall, the relatively complex behavior like steering could be controlled with both extrinsic and intrinsic mechanisms available in this simple model.

Sobinov and Yakovenko

The analysis makes specific predictions about the propriospinal pathways that could be involved in the long-term adaptations to asymmetry. Human subjects could learn to compensate for the external perturbations applied to limbs, while minimizing the overall limb impedance (56,57). Even gross cortical inputs, like those generated by transcortical magnetic stimulation, can be compensated by the adaptation of transmission gains contributing to the regulation of locomotion (58). Our results suggest that this adaptation can take place not only within the pathways projecting to the CPG, but also within the model's limited locus of interactions. While the model has no realistic learning dynamics, the examination was limited to the naïve symmetrical and adapted asymmetrical states. The learning function could be implemented in the future work with the use of simple learning mechanisms (59,60) where the intrinsic parameters could be updated under the reinforcement learning dynamics (61,62). Overall, the model demonstrated that the general locomotor patterns for symmetric and asymmetric gaits may be achieved by the superposition of commands and intrinsic interactions within the minimalistic structure of CPG. This novel flexibility of functional representation for asymmetric pattern generation has not been previously demonstrated in models, and it posits specific predictions for mal- or adaptations to asymmetry due to peripheral or central abnormalities.

The simple model of locomotor rhythm generation

The sensitivity analysis indicates robustness of the current model that it unlikely to be overfitting the behavior. Still, there is the possibility that this model is instead underfitting the locomotor patterns associated with the asymmetric gait. To discuss the appropriate level of abstraction that limits the possibility of underfitting for this task, we need to examine the concept of neuromechanical tuning (63,64). Specifically, the locomotor control is a phenomenon produced by multiple elements that combine predictive and reactive functions. In analogy with the Smith's predictor(21), the specific role of CPG is to predict the

mechanical interactions between the limb and ground. To this extent, our model can reproduce the transformation from input speeds to appropriate inter- and intra-limb coordination of multiple muscle groups (2). The CPG function could then be specified as a dynamical transformation of simple high-level signals into the complex granular functional subdivisions of the temporal activations appropriate for locomotion. Both analytical and numerical solutions of our minimalistic CPG model support the hypothesis that the main function of CPG is the transformation of high-level locomotor signals associated with the whole limb function, i.e. the speed of locomotion, into the low-level phasic activity patterns of limb muscles. This computational inference agrees with the previous studies demonstrating that the one-dimensional input to the mesencephalic locomotor region (MLR) in the form of stimulation magnitude or frequency can be transformed by CPG into the specific velocity-dependent phasic activity in vertebrates (5,65). Thus, the underfitting for CPG models describing the phase duration characteristic would be classified by the inability to use high-level signals related to the forward velocity as the control signals for asymmetric gait. We demonstrated that this model can readily transforms the limb velocity-related inputs into asymmetric phase characteristics. Moreover, the model can embed these high-level representations within its internal structure. And, shown previously (9), it can generate both flexor-dominated and extensor-dominated phase regulation at different speeds.

To conclude, in this paper we report an analytical solution for the bilateral CPG model capable of generating symmetrical and asymmetrical gaits. The asymmetrical behavior can be generated by both the extrinsic inputs to left and right half-center oscillators or the embedded asymmetry within the intrinsic 'propriospinal' gains from extensor half-centers to the contralateral flexor or extensor half-centers. Moreover, these asymmetric changes may correspond either to a natural control of

Sobinov and Yakovenko

small limb velocity adjustments regulating the heading direction or to pathological changes to the inputs or structure of the locomotor CPG.

Acknowledgements

The authors thank Dr. Jonathan Rubin for the general discussion of analytical solutions in locomotor CPG modeling. This work was supported by AS student fellowship NIH/NIGMS U54GM104942, NIH CoBRE P20GM109098 and NIH/NIGMS Centers of Biomedical Research Excellence award U54GM104942.

References

1. Grillner S, Zangger P. How detailed is the central pattern generation for locomotion? *Brain Res.* 1975 May 2;88(2):367–71.
2. Yakovenko S. A hierarchical perspective on rhythm generation for locomotor control. Gossard J-P, editor. *Prog Brain Res. Progress in brain research. Progress in brain research*; 2011;188(10):151–66.
3. Prochazka A, Ellaway P. *Sensory Systems in the Control of Movement*. Hoboken, NJ, USA: John Wiley & Sons, Inc; 2012.
4. Grillner S, Wallén P. Central pattern generators for locomotion, with special reference to vertebrates. *Annu Rev Neurosci.* 1985;8(1):233–61.
5. Shik ML, Severin FV, Orlovskii GN. [Control of walking and running by means of electric stimulation of the midbrain]. *Biofizika.* 1966;11(4):659–66.
6. Cabelguen J-M, Bourcier-Lucas C, Dubuc R. Bimodal locomotion elicited by electrical stimulation of the midbrain in the salamander *Notophthalmus viridescens*. *The Journal of Neuroscience : the official journal of the Society for Neuroscience.* 2003 Mar 15;23(6):2434–9.
7. Verzár F. Reflexumkehr (paradoxe Reflexe) durch zentrale Ermüdung beim Warmbluter. *Pflügers Archiv.* 1923 Dec 31;199(1):109–24.
8. Bashor DP. A large-scale model of some spinal reflex circuits. *Biol Cybern.* 1998 Feb 1;78(2):147–57.
9. Yakovenko S, McCrea DA, Stecina K, Prochazka A. Control of locomotor cycle durations. *J Neurophysiol.* 2005 Aug;94(2):1057–65.
10. Rybak IA, Shevtsova NA, Lafreniere-Roula M, McCrea DA. Modelling spinal circuitry involved in locomotor pattern generation: insights from deletions during fictive locomotion. *J Physiol.* 2006 Dec 1;577(Pt 2):617–39.
11. Markin SN, Klishko AN, Shevtsova NA, Lemay MA, Prilutsky BI, Rybak IA. Afferent control of locomotor CPG: insights from a simple neuromechanical model. *Ann N Y Acad Sci.* 2010 Jun;1198(1):21–34.

Sobinov and Yakovenko

12. Barnett W, Cymbalyuk G. Bifurcation control of gait transition in insect locomotion. BMC Neurosci. 2014.
13. Taga G, Yamaguchi Y, Shimazu H. Self-organized control of bipedal locomotion by neural oscillators in unpredictable environment. Biol Cybern. 1991 Jan 1;65(3):147–59.
14. Brown TG. The intrinsic factors in the act of progression in the mammal. P Roy Soc B-Biol Sci. 1911 Dec 8;84(572):308–19.
15. Grillner S. Comprehensive Physiology. Terjung R, editor. Comprehensive Physiology. Hoboken, NJ, USA: John Wiley & Sons, Inc; 1981.
16. Bonnot A, Whelan PJ, Mentis GZ, O'Donovan MJ. Spatiotemporal pattern of motoneuron activation in the rostral lumbar and the sacral segments during locomotor-like activity in the neonatal mouse spinal cord. The Journal of Neuroscience : the official journal of the Society for Neuroscience. 2002 Feb 1;22(3):RC203.
17. O'Donovan MJ, Bonnot A, Wenner P, Mentis GZ. Calcium imaging of network function in the developing spinal cord. Cell Calcium. 2005 May;37(5):443–50.
18. Yakovenko S, Mushahwar V, VanderHorst V, Holstege G, Prochazka A. Spatiotemporal activation of lumbosacral motoneurons in the locomotor step cycle. J Neurophysiol. 2002 Mar;87(3):1542–53.
19. Hägglund M, Dougherty KJ, Borgius L, Itohara S, Iwasato T, Kiehn O. Optogenetic dissection reveals multiple rhythmogenic modules underlying locomotion. Proc Natl Acad Sci USA. National Acad Sciences; 2013 Jul 9;110(28):11589–94.
20. Kuo AD. The relative roles of feedforward and feedback in the control of rhythmic movements. Motor Control. 2002 Apr 1;6(2):129–45.
21. Smith O. Posicast control of damped oscillatory systems. 1957.
22. Wolpert DM, Ghahramani Z. Computational principles of movement neuroscience. Nat Neurosci. 2000 Nov 1;3 Suppl(suppl):1212–7.
23. Full RJ, Koditschek DE. Templates and anchors: neuromechanical hypotheses of legged locomotion on land. J Exp Biol. 1999 Dec;202(Pt 23):3325–32.
24. Kawato M. Internal models for motor control and trajectory planning. Curr Opin Neurol. 1999 Dec 1;9(6):718–27.
25. Bhushan N, Shadmehr RE. Computational nature of human adaptive control during learning of reaching movements in force fields. Biol Cybern. 1999 Jul 1;81(1):39–60.
26. Wolpert DM, Miall RC, Kawato M. Internal models in the cerebellum. 1998 Sep 1;2(9):338–47. Available from: <http://www.sciencedirect.com/science/article/B6VH9-3TX4M94-6/1/ad0d65770da0595c72df32125d8cb36b>
27. Ijspeert AJ, Nakanishi J, Hoffmann H, Pastor P, Schaal S. Dynamical movement primitives: learning attractor models for motor behaviors. Neural Comput. 2013 Feb;25(2):328–73.

Sobinov and Yakovenko

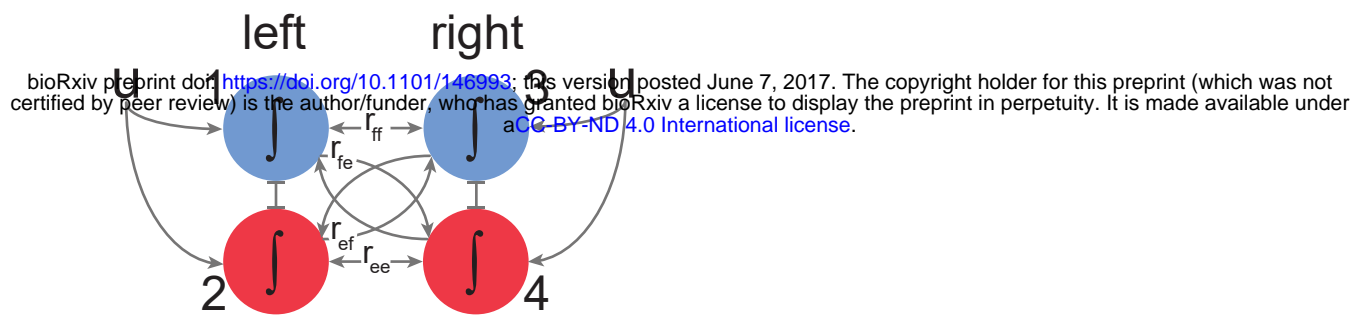
28. Ijspeert AJ. Central pattern generators for locomotion control in animals and robots: a review. *Neural networks : the official journal of the International Neural Network Society*. 2008 May;21(4):642–53.
29. Matsuoka K. Sustained oscillations generated by mutually inhibiting neurons with adaptation. *Biol Cybern*. 1985;52(6):367–76.
30. Schöner G, Jiang WY, Kelso JA. A synergetic theory of quadrupedal gaits and gait transitions. *J Theor Biol*. 1990 Feb 9;142(3):359–91.
31. Wallén P, Ekeberg O, Lansner A, Brodin L, Tråvén H, Grillner S. A computer-based model for realistic simulations of neural networks. II. The segmental network generating locomotor rhythmicity in the lamprey. *J Neurophysiol*. 1992 Dec 1;68(6):1939–50.
32. Cymbalyuk GS, Gaudry Q, Masino MA, Calabrese RL. Bursting in leech heart interneurons: cell-autonomous and network-based mechanisms. *The Journal of Neuroscience : the official journal of the Society for Neuroscience*. 2002 Dec 15;22(24):10580–92.
33. Horn RA, Johnson CR. *Matrix Analysis*. Cambridge, UK: Cambridge University Press; 1999. 2 p.
34. Halbertsma JM. The stride cycle of the cat: the modelling of locomotion by computerized analysis of automatic recordings. *Acta Physiol Scand Suppl*. 1983;521:1–75.
35. Goslow GE, Reinking RM, Stuart DG. The cat step cycle: hind limb joint angles and muscle lengths during unrestrained locomotion. *J Morphol*. 1973 Sep 1;141(1):1–41.
36. Wales DJ, Doye JPK. Global Optimization by Basin-Hopping and the Lowest Energy Structures of Lennard-Jones Clusters Containing up to 110 Atoms. Vol. 101, *The Journal of Physical Chemistry A*. American Chemical Society; 1997. 6 p.
37. Oliphant TE. *Python for Scientific Computing*. Computing in Science Engineering. 2007 Apr 10;9:10–20.
38. Powell MJ. An efficient method for finding the minimum of a function of several variables without calculating derivatives. *The computer journal*. Br Computer Soc; 1964;7(2):155–62.
39. Nocedal J, Wright SJ. *Sequential quadratic programming*. Springer; 2006.
40. Byrd RH, Lu P, Nocedal J, Zhu C. A limited memory algorithm for bound constrained optimization. *SIAM Journal on Scientific Computing*. SIAM; 1995;16(5):1190–208.
41. Frigon A, Thibaudier Y, Hurteau M-F. Modulation of forelimb and hindlimb muscle activity during quadrupedal tied-belt and split-belt locomotion in intact cats. *Neuroscience*. 2015 Apr 2;290:266–78.
42. Barnett WH, Cymbalyuk GS. A codimension-2 bifurcation controlling endogenous bursting activity and pulse-triggered responses of a neuron model. Wennekers T, editor. *PLoS ONE*. 2014;9(1):e85451.
43. Izhikevich EM. Which model to use for cortical spiking neurons? *IEEE Trans Neural Netw*.

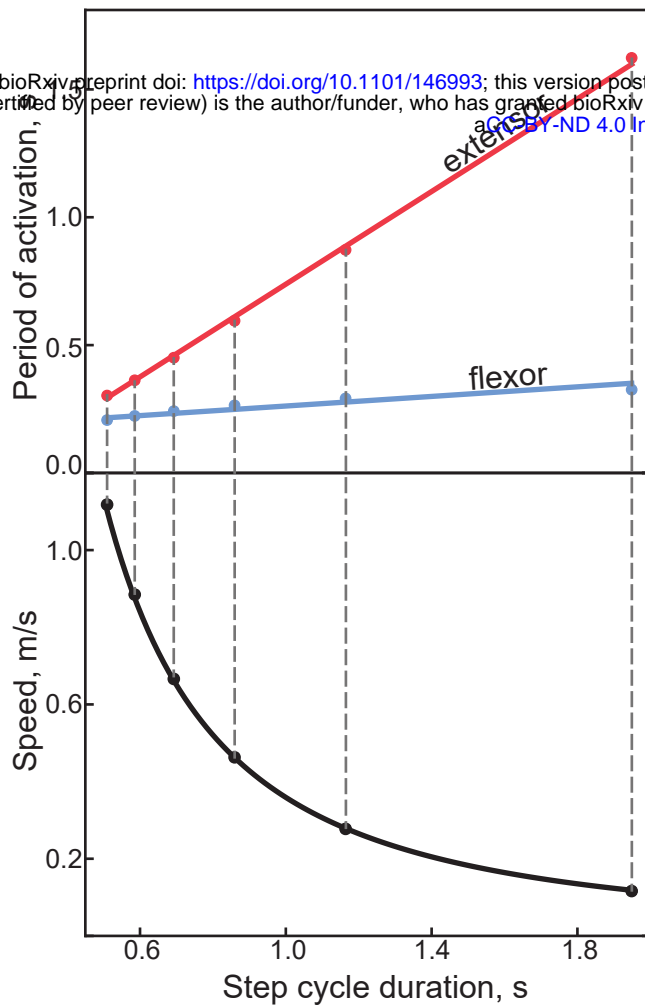
Sobinov and Yakovenko

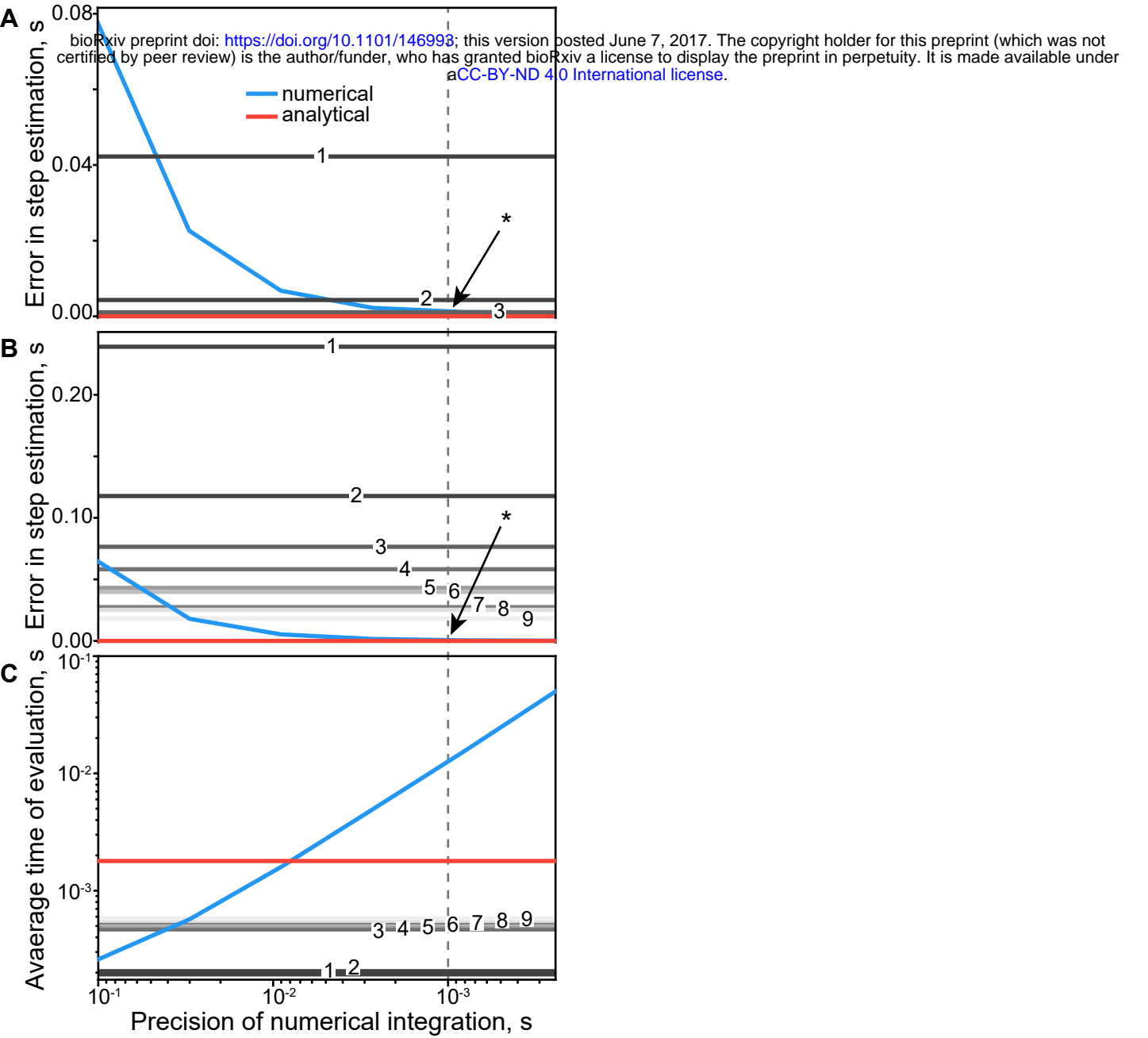
- IEEE; 2004 Sep;15(5):1063–70.
44. Tabak J, Senn W, O'Donovan MJ, Rinzel J. Modeling of spontaneous activity in developing spinal cord using activity-dependent depression in an excitatory network. *The Journal of Neuroscience : the official journal of the Society for Neuroscience*. 2000 Apr 15;20(8):3041–56.
45. Spardy LE, Markin SN, Shevtsova NA, Prilutsky BI, Rybak IA, Rubin JE. A dynamical systems analysis of afferent control in a neuromechanical model of locomotion: II. Phase asymmetry. *J Neural Eng*. IOP Publishing; 2011 Dec;8(6):065004.
46. Spardy LE, Markin SN, Shevtsova NA, Prilutsky BI, Rybak IA, Rubin JE. A dynamical systems analysis of afferent control in a neuromechanical model of locomotion: I. Rhythm generation. *J Neural Eng*. 2011 Dec;8(6):065003.
47. Morris C, Lecar H. Voltage oscillations in the barnacle giant muscle fiber. *Biophys J*. 1981 Jul;35(1):193–213.
48. Caplan JS, Williams AH, Marder E. Many parameter sets in a multicompartment model oscillator are robust to temperature perturbations. *The Journal of Neuroscience : the official journal of the Society for Neuroscience*. Society for Neuroscience; 2014 Apr 2;34(14):4963–75.
49. Lever J, Krzywinski M, Altman N. Points of Significance: Model selection and overfitting. *Nat Meth*. Nature Publishing Group, a division of Macmillan Publishers Limited. All Rights Reserved; 2016 Aug 30;13(9):703–4.
50. Prinz AA, Bucher D, Marder E. Similar network activity from disparate circuit parameters. *Nat Neurosci*. Nature Publishing Group; 2004 Dec;7(12):1345–52.
51. Grashow R, Brookings T, Marder E. Reliable neuromodulation from circuits with variable underlying structure. *Proc Natl Acad Sci USA*. 2009 Jul 14;106(28):11742–6.
52. Goaillard J-M, Taylor AL, Schulz DJ, Marder E. Functional consequences of animal-to-animal variation in circuit parameters. *Nat Neurosci*. 2009 Nov 1;12(11):1424–30.
53. Galbreath K, Olesh E, Yakovenko S. Do humans use limb velocity signal to control locomotion? In: Washington, D.C. 2014.
54. Kiehn O. Development and functional organization of spinal locomotor circuits. *Curr Opin Neurol*. 2011 Feb;21(1):100–9.
55. Hase K, Stein RB. Turning strategies during human walking. *J Neurophysiol*. 1999 Jun;81(6):2914–22.
56. Shadmehr RE, Mussa-Ivaldi FA. Adaptive representation of dynamics during learning of a motor task. *The Journal of Neuroscience : the official journal of the Society for Neuroscience*. 1994 May 1;14(5 Pt 2):3208–24.
57. Dingwell JB, Mah CD, Mussa-Ivaldi FA. Manipulating objects with internal degrees of freedom: evidence for model-based control. *J Neurophysiol*. 2002 Jul 1;88(1):222–35.

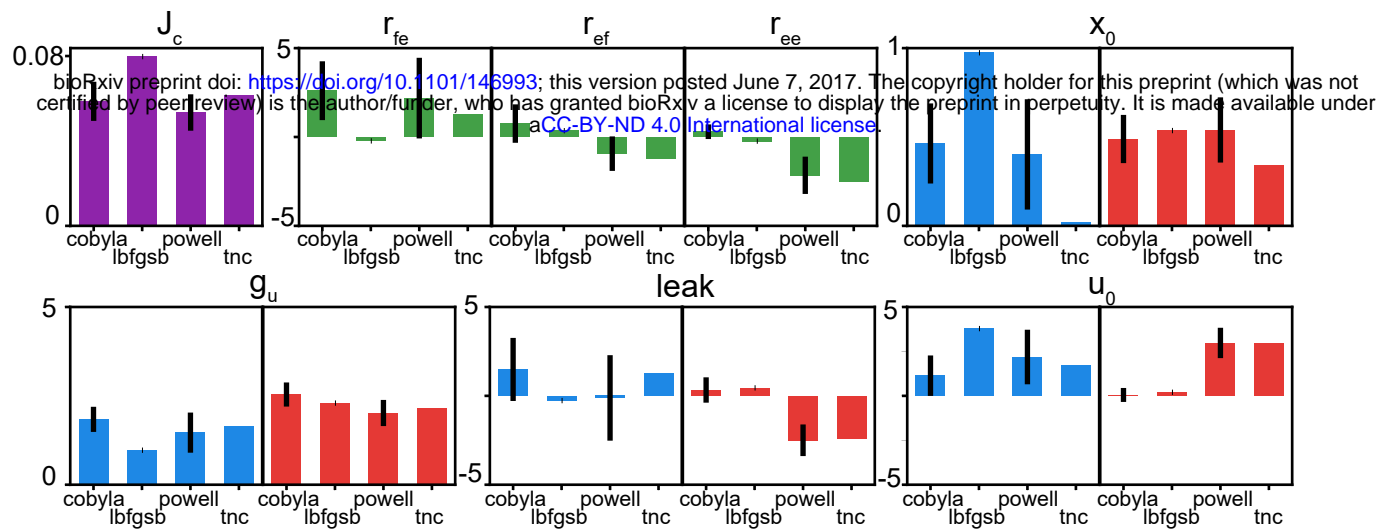
Sobinov and Yakovenko

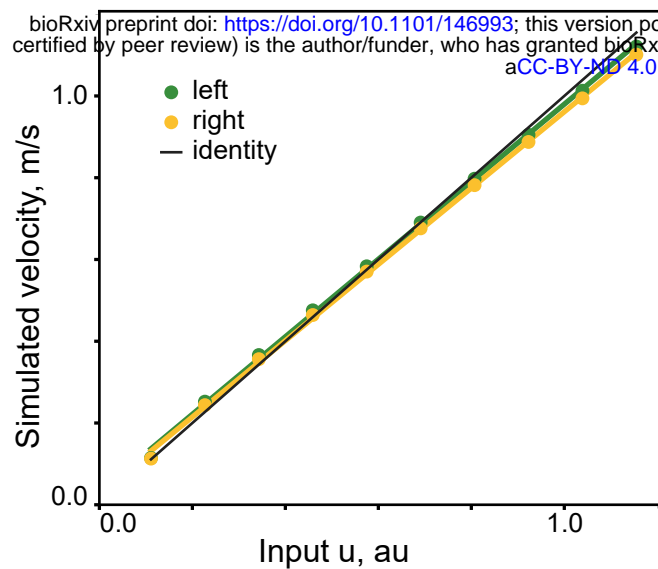
58. Schubert M, Curt A, Colombo G, Berger W, Dietz V. Voluntary control of human gait: conditioning of magnetically evoked motor responses in a precision stepping task. *Exp Brain Res.* 1999 Jun;126(4):583–8.
59. Franklin DW, Burdet E, Tee KP, Osu R, Chew C-M, Milner TE, et al. CNS learns stable, accurate, and efficient movements using a simple algorithm. *The Journal of Neuroscience : the official journal of the Society for Neuroscience.* 2008 Oct 29;28(44):11165–73.
60. Wu HG, Miyamoto YR, Castro LNG, Olfeczký BP, Smith MA. Temporal structure of motor variability is dynamically regulated and predicts motor learning ability. *Nat Neurosci.* 2014 Feb;17(2):312–21.
61. Mahmoudi B, Pohlmeier EA, Prins NW, Geng S, Sanchez JC. Towards autonomous neuroprosthetic control using Hebbian reinforcement learning. *J Neural Eng.* 2013 Dec;10(6):066005.
62. Schultz W. Updating dopamine reward signals. *Curr Opin Neurol.* 2013 Apr;23(2):229–38.
63. Prochazka A, Yakovenko S. The neuromechanical tuning hypothesis. *Prog Brain Res.* Elsevier; 2007;165:255–65.
64. Ting LH, Chiel HJ, Trumbower RD, Allen JL, McKay JL, Hackney ME, et al. Neuromechanical Principles Underlying Movement Modularity and Their Implications for Rehabilitation. *Neuron.* Elsevier Inc; 2015 Apr 8;86(1):38–54.
65. Smetana R, Juvin L, Dubuc R, Alford S. A parallel cholinergic brainstem pathway for enhancing locomotor drive. *Nat Neurosci.* 2010 Jun;13(6):731–8.





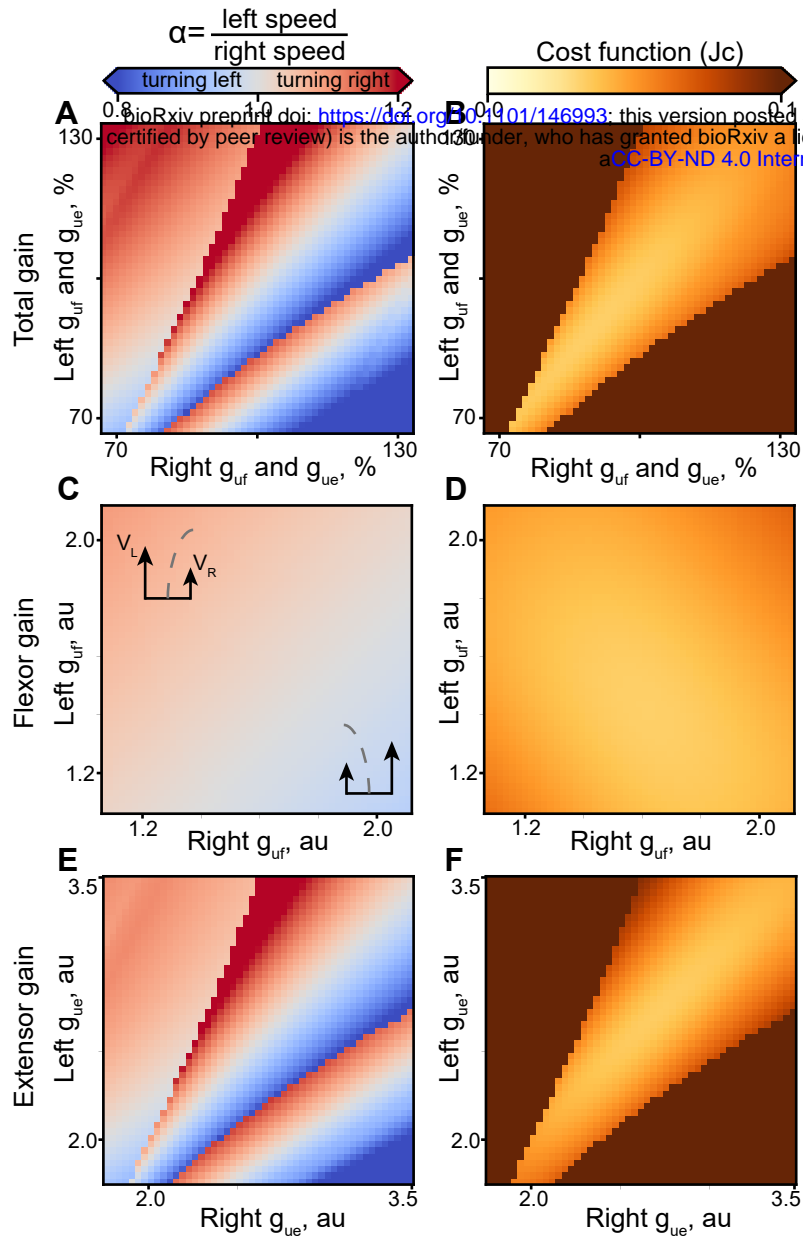






$$\alpha = \frac{\text{left speed}}{\text{right speed}}$$

turning left turning right



$$\alpha = \frac{\text{left speed}}{\text{right speed}}$$

turning left turning right

reduced cost function

